Soils and Foundations 2012;52(5):975–986

The Japanese Geotechnical Society

Soils and Foundations

www.sciencedirect.com
journal homepage: www.elsevier.com/locate/sandf

Slope failures in residential land on valley fills in Yamamoto town

M. Hyodo[a], R.P. Orense[b,*], S. Noda[a], S. Furukawa[c], T. Furui[d]

[a]*Department of Civil & Environmental Engineering, Yamaguchi University, Japan*
[b]*Department of Civil & Environmental Engineering, University of Auckland, New Zealand*
[c]*Frontier Project Section, Chuden Engineering Consultants Co. Ltd., Japan*
[d]*Etajima City Office, Hiroshima Prefecture, Japan*

Received 12 October 2011; received in revised form 18 June 2012; accepted 12 July 2012
Available online 4 December 2012

Abstract

As a result of the 2011 off the Pacific Coast of Tohoku Earthquake, five slope failures occurred in a residential area on artificial valley fills in Taiyo New Town, Yamamoto, Miyagi Prefecture. The site was constructed by leveling a hilly area and using the cut materials as fill for the valleys to provide foundation ground for houses. The fill material was sandy and was derived from the weathering of tuffaceous sandstone which had formed the natural ground. Each of the five slope failures was observed to have occurred either at the edge of the artificial valley fills or within the embankment sections that had been widened for road construction. Laboratory tests show that the fill, which had a fines content of F_c=20%, had a very low liquefaction resistance, which further decreased with the application of initial shear stress. A pseudo-static slope stability analysis, using conventional strength parameters, could not explain the slope failure at one of the sites that failed, but it could explain the slope failure when the dynamic strength was used to represent the soil strength at the slip surface. Thus, the slope failures in Taiyo New Town, at least at the one site analyzed in this study, could be attributed to the liquefaction of the fill material induced by the intense shaking.

Keywords: Earthquake; Slope failure; Valley fill; Pseudo-static analysis; Tuffaceous sandstone; Liquefaction; The off the Pacific coast of Tohoku Earthquake

1. Introduction

With a moment magnitude of M_w 9.0, the gigantic 2011 off the Pacific coast of Tohoku Earthquake caused extensive damage to life and property in the Tohoku and Kanto regions of the eastern part of Japan. Aside from the devastation caused by the large-scale tsunami generated by the earthquake, many slope failures occurred in artificial valley fills in sloping residential lands. Newspaper reports indicated that as many as 950 slope failures in nine prefectures occurred in such valley fills (Asahi Shinbun, 5/23/11 issue). Fig. 1 shows the region in Sendai City where most of the slope failures occurred.

Although located south of this zone, the town of Yamamoto also had its share of earthquake-induced damage. Almost 24 km^2 of the town's 64 km^2 area, or about 38%, was flooded and destroyed by the large-scale tsunami generated by the earthquake (GSI, 2011). Most of the inundated area was on the eastern side of National Route 6 (see Fig. 1). In addition, several slope failures occurred in the hilly areas located to the west of Route 6. In terms of slope failures, one of the worst-hit areas was Taiyo New

*Corresponding author.
E-mail address: r.orense@auckland.ac.nz (R.P. Orense).
Peer review under responsibility of The Japanese Geotechnical Society.

Production and hosting by Elsevier

0038-0806
http://dx.doi.org/10.1016/j.sandf.2012.11.015

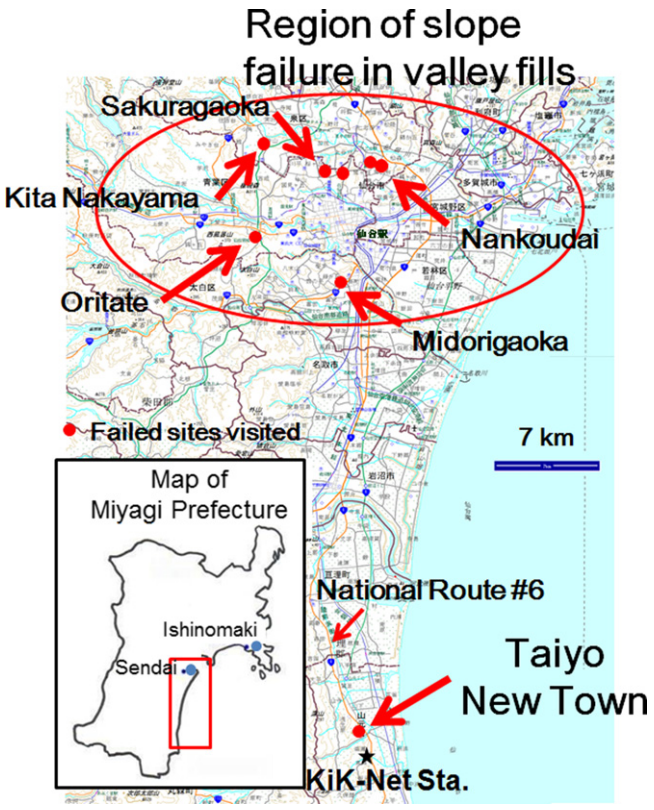

Fig. 1. Map showing location of Taiyo New Town, Yamamoto, as well as other sites of failed slopes.

Town, a housing site located on artificial valley fills just to the west of Route 6. The site was constructed by leveling the hilly area and using the cut materials as fill for the valleys in order to provide viable land for residential purposes. Following the earthquake and its major aftershocks, slope failures occurred in five different sections of the land, damaging houses, roads, a park and pipelines. At one of the failed sites, the debris slid and covered a parking lot just on the side of Route 6.

In the months that followed, site investigations were performed by the authors in order to clarify the causes(s) of the slope failures. Unfortunately, no information was available regarding the original design of the residential site, and therefore, a check of the adequacy of the factor of safety adopted for the fills could not be performed. Instead, the characteristics of the recorded ground motion from a nearby seismic station were analyzed and microtremor measurements were performed to characterize the soil structure in the area. Moreover, samples were obtained at several locations adjacent to the failed slopes, and laboratory tests were conducted to investigate their geotechnical properties. Finally, a slope stability analysis was conducted in order to better understand the response of one of the embankments to earthquake loading. The results highlighted the seismic vulnerability of the residential areas built on the artificial valley fills, like Taiyo New Town, that were constructed with weak tuffaceous materials.

2. Description of the area

The Taiyo New Town housing site is located at the central part of Yamamoto, a coastal town on the southern edge of Miyagi Prefecture, as shown in Fig. 1. It is located in a hilly region to the west of Route 6, which traverses the prefecture in an almost north–south direction. In fact, Route 6 appears to be the dividing line between the coastal plain on the east and the 40–50-m-high mountains (Wariyama uplift zone) on the west of the prefecture.

The site of the residential area was developed in the 1970s by cutting and leveling off some parts of the hills and using the excavated materials as fill for the valleys. Fig. 2 shows the depth distribution of the cuts and fills in Taiyo New Town. To level off the residential land, cuts as high as 10–15 m were made on the hills, while valley floors, as deep as 15–20 m, were filled up using the materials cut from the elevated regions. It can be observed that deep valleys existed in the central portion and along the western boundary of the site. The eastern side of the site adjacent to Route 6 was also filled up to provide road access to the site. The elevation of the filled-up residential site was about 35 m above mean sea level, with a typical fill inclination of 1:1.5, except in sections near Route 6 where the inclination was made safer at 1:1.8. The residential site has an area of about 0.12 km^2, and when the earthquake struck, more than 200 houses had been built at the site.

An investigation of the local geology of the site revealed that the original ground consisted of tuffaceous sandstone of the Yamamoto Formation. Subsequent boring data showed that the sandstone was weakly consolidated and exhibited a high degree of weathering towards the surface, with the surficial layer turning into sandy soil. Thus, the material used to fill up the valleys consisted of sandy soil from the weathered tuffaceous sandstone. Standard penetration tests indicated that the sandy material used as fill had an average N-value of 5, while the highly weathered top layer and the weathered layer of sandstone had average N-values of 6 and 16, respectively.

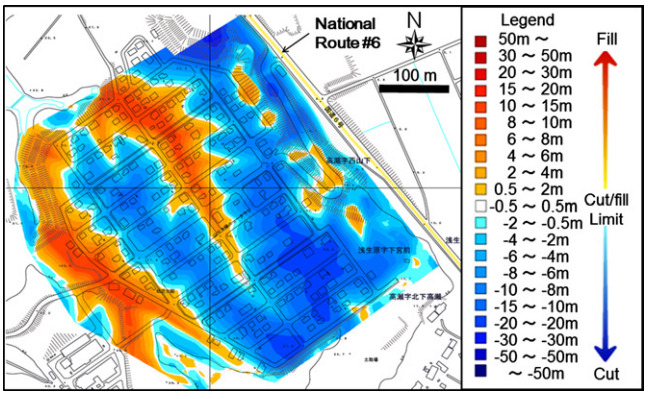

Fig. 2. Housing site foundation map of Taiyo New Town, showing thickness distribution of cut and fill sections (Fukken Gijutsu Consultant, 2008).

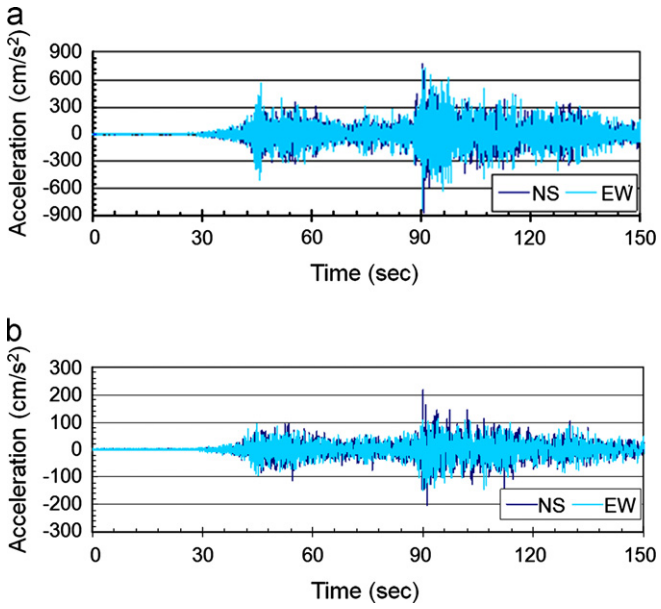

Fig. 3. Acceleration time histories obtained from Yamamoto KiK-Net seismic station: (a) at ground surface and (b) at GL-205 m (data from KiK-Net, 2011).

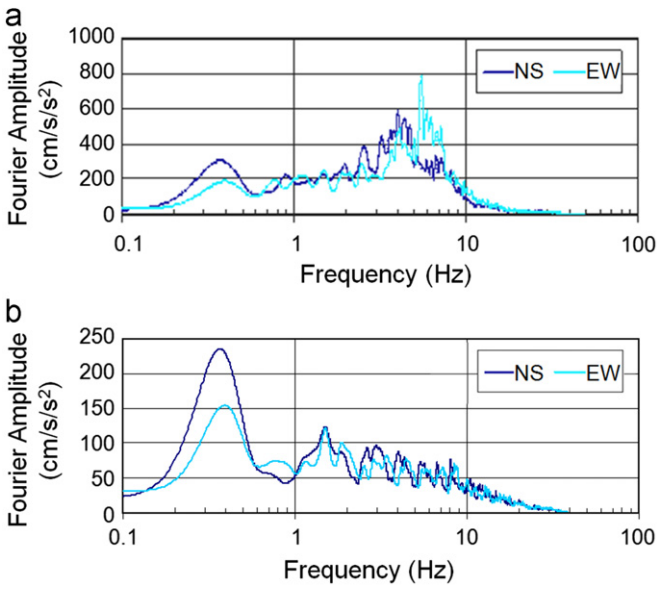

Fig. 4. Fourier spectra of acceleration records obtained from Yamamoto KiK-Net seismic station: (a) at ground surface and (b) at GL-205 m.

3. Strong motion station and seismic records

About 2 km to the south of Taiyo New Town (see Fig. 1), the National Research Institute for Earth Science and Disaster Prevention (NIED) operates a KiK-Net seismic station (MYGH10: Yamamoto Station) with digital strong-motion seismometers installed on the ground surface and at a depth of GL-205 m. The 2011 Tohoku earthquake triggered many seismic stations in the area, including the one in Yamamoto, and recorded strong motions. Fig. 3 shows the acceleration time histories recorded at the station, both on the surface and at a depth of GL-205 m, while Fig. 4 illustrates the corresponding Fourier spectra of the acceleration records. The peak accelerations recorded at a depth of GL-205 m were in the range of 150–220 cm/s^2 with a predominant frequency of 0.35 Hz. On the ground surface, on the other hand, the peak values were much higher, 850–870 cm/s^2, with the predominant frequency shifting to 4–6 Hz. The duration of significant shaking was rather long, about 120 s.

The soil profile at KiK-Net Yamamoto Station is shown in Table 1. It can be observed that tuffaceous sandstone with a shear wave velocity of $V_s < 770$ m/s exists in the vicinity of the seismometer installed at the bottom of the borehole. Moreover, the upper layer generally consists of pumiceous tuff and tuffaceous sandstone. This profile amplified the seismic motion as it propagated towards the ground surface.

4. Outline of damage

Following the 2011 earthquake and its major aftershocks, slope failures occurred at five sites within the Taiyo New Town housing site. The locations of the slope failures are shown in Fig. 5. These failed or slid blocks were sequentially numbered, starting with Failed Block 1, which destroyed the road along the eastern boundary of the housing site, going counterclockwise to Failed Block 5 on the western side. Block 1 consisted of two landslides, referred to as Block 1–1 and Block 1–2.

Comparing the locations of the failed blocks at the housing site (Fig. 5) with the foundation ground map shown in Fig. 2, it is clear that failed Blocks 1 and 2 occurred in the section of fills which was widened to construct the road, while Blocks 3, 4 and 5 occurred along the edge of the valley fills. This suggests that the fill material, rather than the natural ground, was involved in the slope failures.

4.1. Failed block 1

Block 1 consisted of two slope failures. The first sliding block, Block 1–1, caused settlement at the crest and laterally flowed down the sloping ground, as shown in Fig. 6(a). As a result, a house located on the laterally moving ground tilted and a 1-m-high vertical offset was created at the crest. The block was about 54 m wide, 80 m long and 6.7 m deep. Extensional cracks were also observed in the ground and the road pavements. The adjacent failed block, Block 1–2, was smaller in scale (40 m wide, 31 m long and 6.3 m deep) and induced cracking in the road as the sliding mass moved. In both cases, the surface of the road's downslope was pushed up as a result of the movement. The embankment was widened at this site for the purpose of road construction. Fig. 6(b) and (c) show the cross-sectional profiles of Blocks 1–1 and 1–2, respectively.

4.2. Failed block 2

About 50 m north of failed Block 1, the shoulder of an embankment collapsed, sending debris 15 m below towards

Table 1
Soil profile at Yamamoto KiK-Net seismic station (MYGH10) (data from KiK-Net website).

Depth to layer bottom (m)	Thickness (m)	Type of soil/rock	V_p (m/s)	V_s (m/s)
2.0	2.0	Clay	500	110
3.5	1.5	Clay	1750	250
8.0	4.5	Sandstone	1750	390
18.0	10.0	Conglomerate	1750	390
34.0	16.0	Sandstone	1750	390
42.0	8.0	Pumiceous tuff	1830	590
114.0	72.0	Tuffaceous sandstone	1830	590
142.0	28.0	Sandstone	1920	770
178.0	36.0	Tuffaceous sandstone	1920	770
208.0	30.0	Silt	1920	770

Fig. 5. Location of failed slopes at Taiyo New Town residential site.

the parking lot adjacent to a convenience store (see Fig. 7(a)). It is apparent that the failure was confined to the upper layer consisting of fill material. A house located at the crest of the sliding mass was partially destroyed, while the roads positioned at the top and the midway of the slope were totally destroyed, sending cracked pavements downward. The cross-sectional profile of the slope is shown in Fig. 7(b). Block 2 is also located in a section of the embankment which was widened to accommodate the road. The retaining wall in this area (adjacent to the location of the left boring log in the figure) collapsed as a result of the failure. The bottom retaining wall (to the left of the figure near the main road) remained standing, but was covered with debris. Just to the north of the failed slope and down on the main road, a reinforced retaining wall missed the landslide. This particular retaining wall was constructed in 2008 when the section failed following a heavy rainfall; the retaining wall was not damaged by this earthquake.

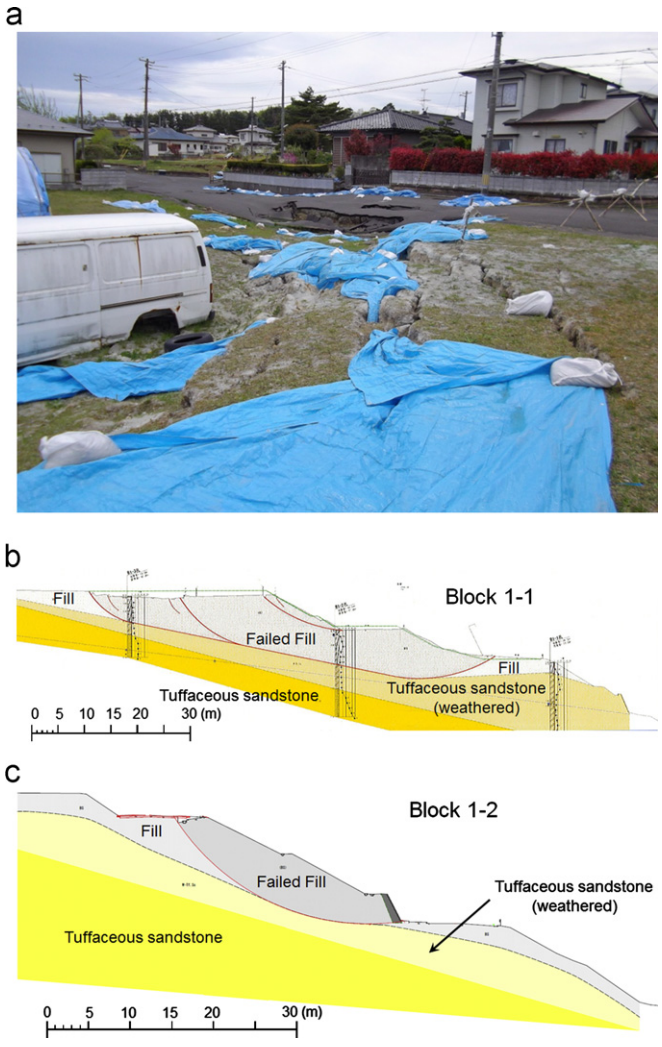

Fig. 6. (a) View of crest at failed slope in Block 1–1 showing extensional cracks and vertical offsets, (b) cross-sectional profile of failed slope in Block 1–1 and (c) cross-sectional profile of failed slope in Block 1–2.

4.3. Failed block 3

The third failed block, Block 3, is located on the northern edge of the slope adjacent to a steep ravine. In this section,

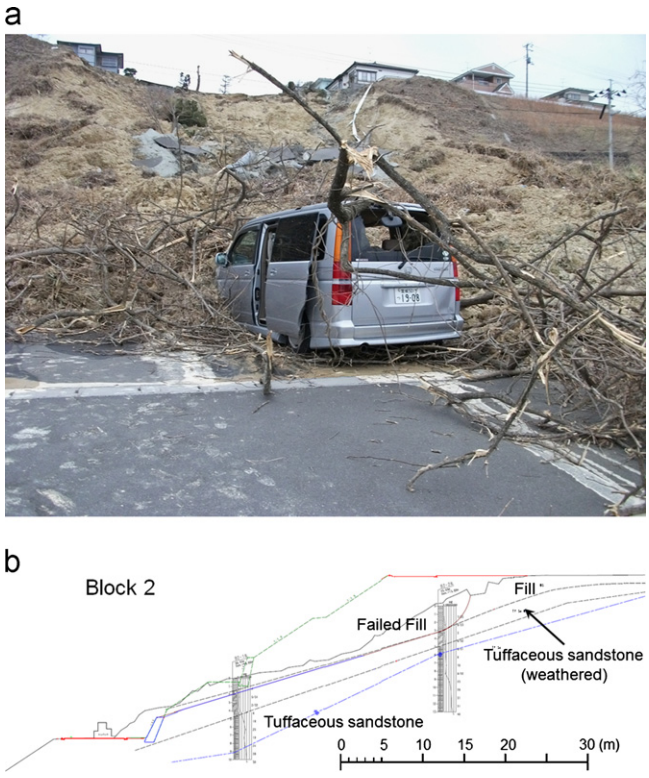

Fig. 7. (a) View of slope failure in Block 2 from parking lot below and (b) cross-sectional profile of failed slope in Block 2.

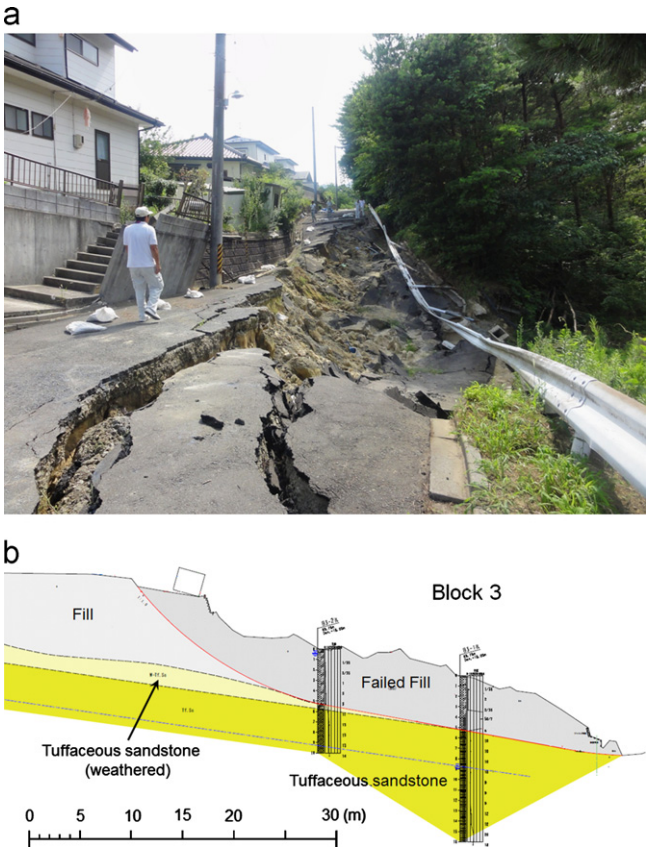

Fig. 8. (a) View at top of failed slope in Block 3 (at least three houses were affected by movement and extensional cracks that developed) and (b) cross-sectional profile of failed slope in Block 3.

a portion of the road embankment collapsed over a distance of 15–20 m, and the fill materials flowed down the slope. Fig. 8(a) shows the condition of the failed slope, while Fig. 8(b) depicts the cross-sectional profile of the slope. A house adjacent to the road and located on top of the crest tilted, together with the fence and road railings. Vertical offsets in the order of 20–30 cm were observed near the house, exposing its foundation and leaving the house hanging precariously on its edge. Extensional ground cracks were also observed near two other houses. Moreover, the debris blocked drainage channels installed in the middle of the slope. The end of the embankment was reinforced with gabions; however, the gabions failed together with the embankment.

4.4. Failed block 4

The fourth failed block, Block 4, occurred on the west corner of the housing site. A small park was located at the crest of the failed slope, and some playground facilities tilted due to the lateral movement of the ground. Cracks, with openings as wide as 10–20 cm, crisscrossed the surface of the park (Fig. 9(a)). Under such conditions, the playground was deemed unsafe. In a nearby road, cracks and vertical offsets were visible. A large crack was also observed adjacent to a manhole, exposing the structure. Some U-shaped channels were seen in the middle of the failed slope, presumably coming from the top section of the road. A concrete block retaining wall, installed at the toe of the embankment, collapsed as a result of the failure. Fig. 9(b) illustrates the estimated cross-sectional profile of the slope.

4.5. Failed block 5

Fig. 10(a) shows the fifth failed block, Block 5, in the western section of the site. A two-story house on top of the slope was damaged due to vertical offsets and extensional failure resulting from slope movement. The house was tilted, exposing its foundation. Fences, railings and other lightweight structures also collapsed. The road on the crest of the failed slope subsided and the debris covered the drainage channels. Portions of road pavements, as well as damaged sewage facilities, were seen among the flowed debris. The soil debris was observed to consist of sand and sandy soil, representing the material of the fill. Fig. 10(b) shows the cross-sectional profile of the slope.

5. Soil and site characteristics

To understand the characteristics of the fill material, soil samples were obtained adjacent to the failed blocks and geotechnical laboratory tests were performed. In addition,

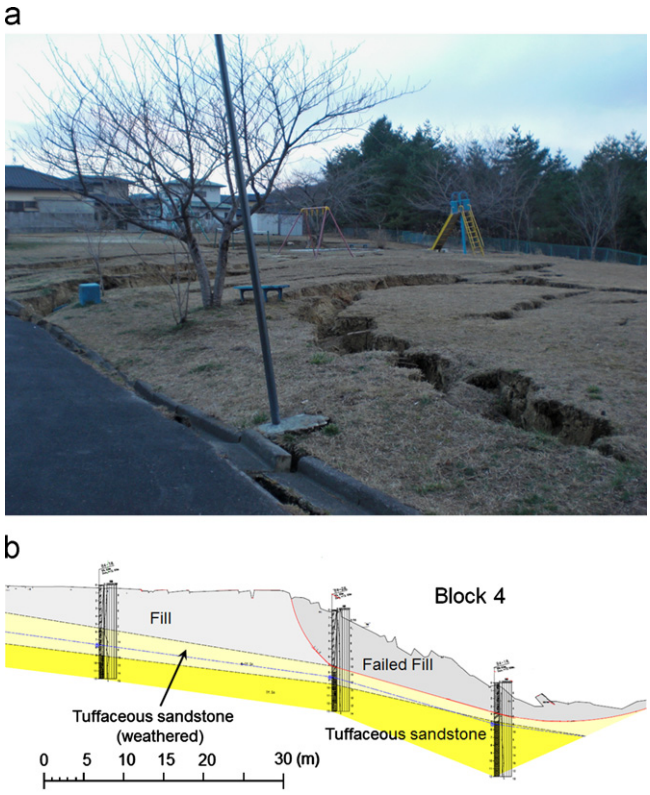

Fig. 9. (a) Extensional cracks at park located on crest of failed slope in Block 4 (failure was toward right of photo) and (b) cross-sectional profile of failed slope in Block 4.

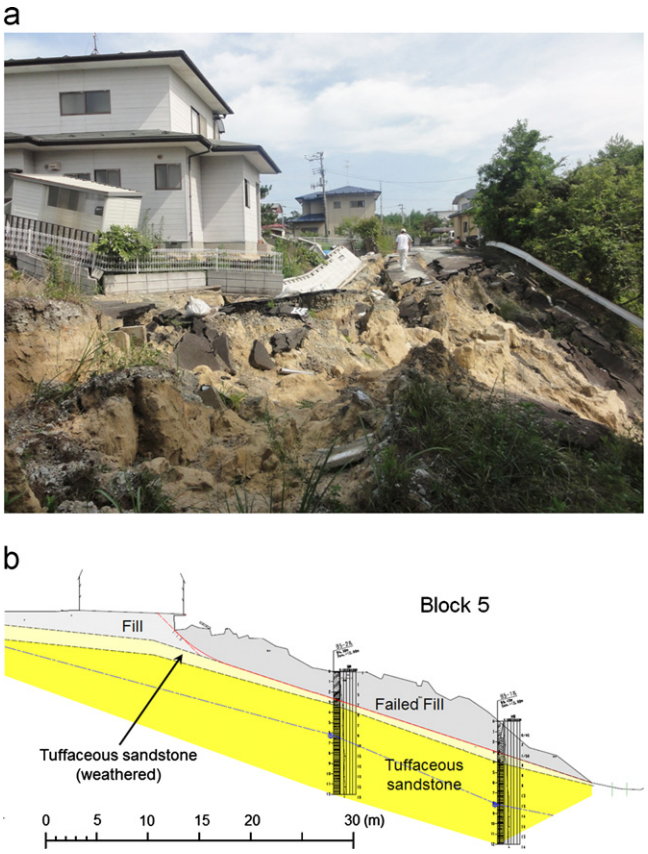

Fig. 10. (a) View of slope failure in Block 5 (house hangs precariously on edge of failed slope) and (b) cross-sectional profile of failed slope in Block 5.

microtremor measurements were conducted near the failed slopes to determine the natural period of the embankment.

5.1. Geotechnical properties

Soils samples were obtained near the failed blocks in order to investigate the geotechnical properties of the soil used as fill. Fig. 11 shows the grain size distribution curves for the samples from the three sites. It can be seen that the curves are fairly similar for all four locations, indicating that the fill materials were similar throughout the housing site. The soil has a well-graded grain size distribution with a fines content of $F_c=20\%$.

Samples obtained from the Block 2 site were quite abundant and they were used in most of the geotechnical laboratory tests. Index property tests, based on Japanese Geotechnical Society standards (JGS, 2000), showed that the density of the particles was 2.478 g/cm^3, while the maximum and minimum densities were 1.319 and 1.079 g/cm^3, respectively. Note that the latter values are quite small; a possible reason is that maximum and minimum density tests are designed for granular soils, not fine soils, especially ones with a fines content of $F_c=20\%$. A compaction curve is shown in Fig. 12, where it is seen that the optimum water content is $w_{opt}=13.8\%$, corresponding to a maximum dry density of $\rho_{dmax}=1.822$ g/cm^3.

Next, monotonic drained and cyclic undrained triaxial tests were conducted on the soil samples. In these tests, the

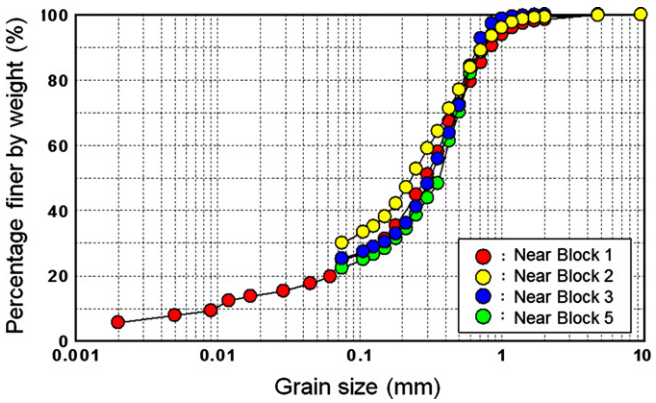

Fig. 11. Grain size distribution curves of samples obtained from four locations.

reconstituted samples were prepared by the moist tamping method and tamped sufficiently such that the dry density was equal to 90% of the maximum dry density, i.e., a degree of compaction of $D_c=90\%$. Using the obtained maximum and minimum dry densities, this corresponds to a relative density of $D_r=188\%$. The results of the monotonic drained tests for confining pressure levels of $\sigma_c'=50$, 100 and 150 kPa are shown in Fig. 13. The soil shows contractive behavior at all levels of applied pressure.

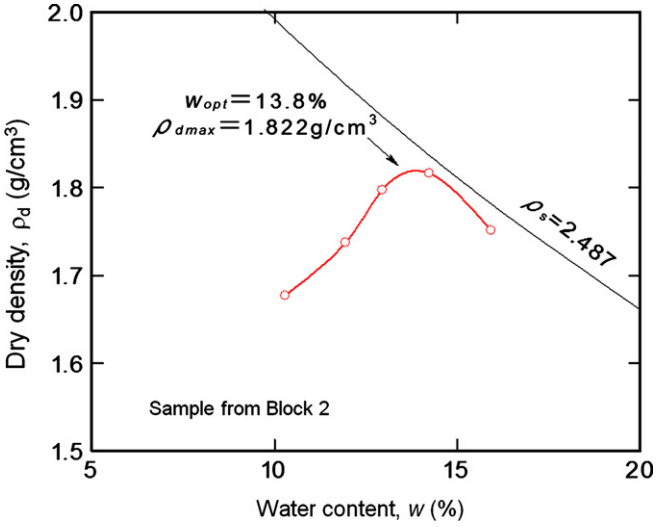

Fig. 12. Compaction curve for Block 2 samples.

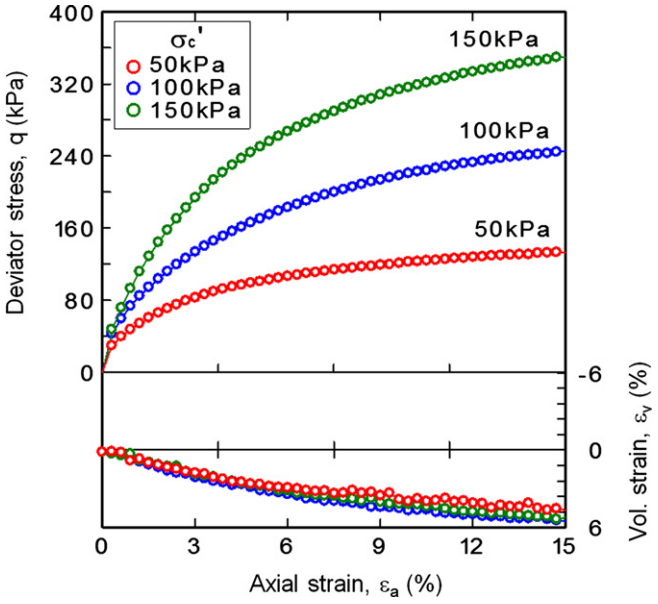

Fig. 13. Results of consolidated drained triaxial tests.

From the stress-strain relations, Mohr circles of stress were drawn at the residual state and the strength parameters were obtained. The results indicate the following values: cohesion $c'=9$ kPa and angle of internal friction $\phi'=31.7^{\circ}$. Such an internal friction angle is considered low for this type of dense sandy soil.

Cyclic undrained triaxial tests were performed on reconstituted samples under isotropically consolidated conditions. The obtained liquefaction resistance curve, corresponding to a double amplitude axial strain of $\varepsilon_{DA}=5\%$, is shown by the solid circles in Fig. 14. It is seen that the liquefaction resistance of the material is quite low, indicating the susceptibility of the material to large deformation when shaken under saturated conditions. This may be due to the high proportion of non-plastic fines in the soil, which can decrease the liquefaction

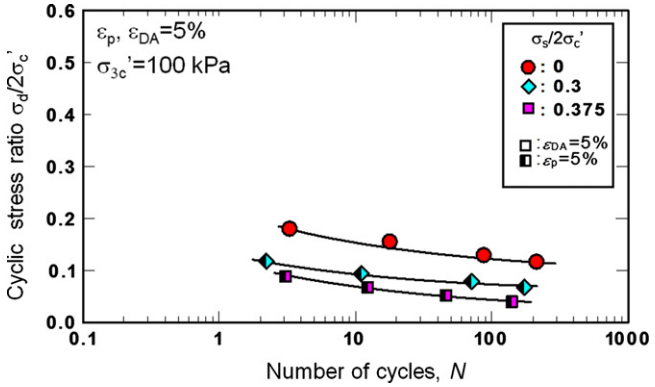

Fig. 14. Liquefaction resistance curves of isotropically and anisotropically consolidated samples.

resistance (Hyodo et al., 2006), and to the density used to prepare the reconstituted specimens. Note that for soil specimens with a degree of compaction of $D_c=90\%$, the dry density of the soil was taken as 1.64 g/cm^3. According to the Yamamoto Town Office, dry densities ranging from 1.44–1.54 g/cm^3 were obtained at the site based on previous site investigations. Thus, although the density of the specimen used in the test was higher than the in situ values, the liquefaction resistance of the soil was low. Although the location of the water table during the earthquake was not confirmed, this type of material will liquefy easily when subjected to cyclic shearing induced by an earthquake, and will fail due to the reduction in effective stress.

In order to simulate the presence of initial shear stress in sloping grounds, such as in the present embankment, cyclic undrained triaxial tests were also performed on anisotropically consolidated specimens. Results for cases with initial shear stress ratios of $\sigma_s/2\sigma_c'=0.30$ ($\sigma_s/2\sigma_{3c}'=0.375$) and $\sigma_s/2\sigma_c'=0.375$ ($\sigma_s/2\sigma_{3c}'=0.5$) are also indicated in Fig. 14, wherein σ_s is the initial deviator stress, σ_c' is the mean effective principal stress at the end of anisotropic consolidation and σ_{3c}' is the lateral cell pressure. In the case of the anisotropically consolidated samples, the liquefaction resistance was defined in terms of a peak axial strain $\varepsilon_p=5\%$. It appears that when the fill material is subjected to initial static shear stress, the liquefaction resistance further decreases; such behavior is quite different from that observed for other types of granular material where liquefaction resistance increases with the application of initial shear stress (Vaid et al., 1990; Hyodo et al. 1991, 1994; Hosono and Yoshimine, 2004). This confirms that the fill material is indeed weak and susceptible to large deformation under undrained earthquake loading.

Fig. 15 shows the stress paths and the stress–strain relations for the cases of $\sigma_s/2\sigma_c'=0$, 0.30 and 0.375. It can be observed that in all cases, the effective stress did not decrease to zero; however, large deformation suddenly developed after a certain number of loadings. This is more pronounced in the cases of $\sigma_s/2\sigma_c'=0.30$ and 0.375. Thus, in both cases, failure occurred as a result of large deformation.

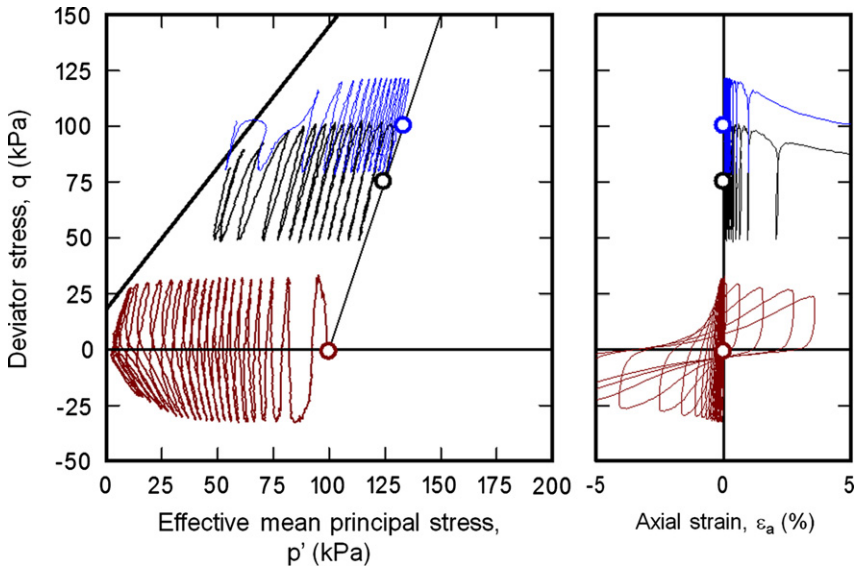

Fig. 15. (a) Stress paths and (b) stress–strain relations for cases of $\sigma_s/2\sigma_c'=0$, 0.30 and 0.375.

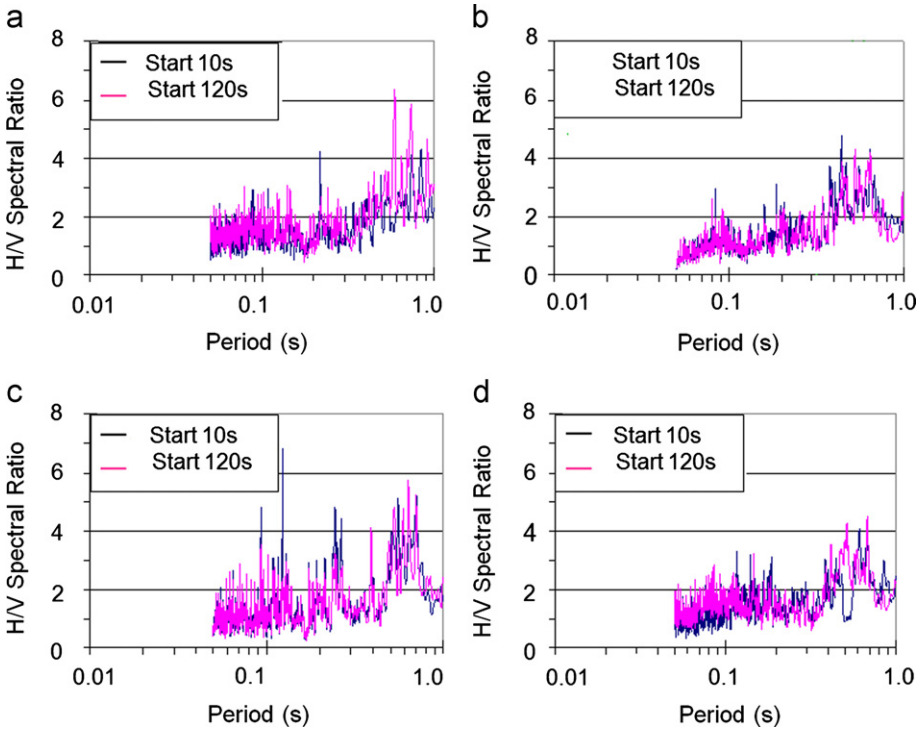

Fig. 16. Horizontal-to-vertical (H/V) spectral ratios obtained from microtremor measurements. (a) Near Block 1, (b) Near Block 3, (c) Near Block 5 and (d) South of Block 5.

5.2. Microtremor measurements

To determine the natural period and other dynamic characteristics of the fill, microtremor measurements were conducted on top of the embankment near the location of the failed slopes. This method does not require any boreholes and is more convenient and cheaper than the traditional borehole method. Plots of the horizontal-to-vertical (H/V) spectral ratio of microtremors at each site are shown in Fig. 16. The plots were done at two time intervals, corresponding to the data recorded from $t=10$ s and from $t=120$ s. Then, the method proposed by Nakamura (1989) was used, in which it is assumed that the source effect can be minimized by normalizing the horizontal spectral amplitude (H) with the vertical spectral amplitude (V) and that the shear wave dominates the microtremor; this results in the H/V peak period and peak value itself corresponding to the natural site period and amplification factor, respectively. Thus, from the obtained H/V peak period, the corresponding natural site period was calculated. The results, summarized in

Table 2
Peak period of H/V spectral ratios obtained at each microtremor site.

Site	Peak period (s)		
	Interval starting at 10 s	Interval starting at 120 s	Average value
1—Near Block 1	0.836	0.589	0.71
3—Near Block 3	0.442	0.648	0.54
4—Near Block 5	0.706	0.635	0.67
5—South of Block 5	0.614	0.683	0.65

Table 2, show that all four points where the slope failures occurred have relatively long periods, i.e., greater than 0.5 s, indicating that the soft deposits are generally thick in these areas.

6. Slope stability analyses

To explain the cause of failure, a preliminary analysis was conducted considering the stability of the embankments during the 2011 earthquake under different scenarios. For this purpose, a pseudo-static slope stability analysis was performed at the Block 1 site. The equivalent strong motion at the top of the embankment (Point A) was determined from the motion at the engineering bedrock (Point C) through the procedure outlined in Fig. 17. Firstly, the model for the 1-D soil profile at the location of the KiK-Net seismic station (Table 1) was verified using earthquake recordings obtained during the previous smaller earthquakes of 1 September 2010 ($PGA_{NS}=2.5$ cm/s^2, $PGA_{EW}=3.1$ cm/s^2) and 10 February 2011 ($PGA_{NS}=4.6$ cm/s^2, $PGA_{EW}=3.8$ cm/s^2). This was necessary in order to check if the small-strain moduli used in the analysis could result in a good simulation of the recorded motions. In both cases, the time history of the acceleration recorded on the ground surface was used as input and the acceleration at the bottom of the borehole (GL-205 m) was simulated using the equivalent linear program SHAKE (Schnabel et al., 1972). The resulting simulations, although not given here, showed very similar time histories and Fourier spectra of the at-depth accelerations when compared with the recorded motions.

After confirming that the model worked well for small-amplitude earthquakes, the non-linear response of the soil, due to the larger amplitude of motion resulting from the 2011 Tohoku earthquake event, was considered next, along with the surface motion (Fig. 3(a)) used as input to simulate the motion at GL-205 m (Fig. 3(b)). Due to space limitations, details of the calculations are not presented here. Suffice it to say that the 1-D ground model at the seismic station site was sufficiently validated. From the analysis using the 2011 ground motions, the outcrop motion (2E) at the engineering bedrock, Point C, was calculated for both N–S and E–W directions.

For the purpose of analysis, the cross-sectional profile for Block 1–1, shown in Fig. 6(b), was used. Using the boring data obtained from field tests and knowing that the natural period of the site is 0.7 s (see Table 2), the soil profile and corresponding parameters were established, as summarized in Table 3. The depth of the engineering bedrock from the surface of the fill was 34 m.

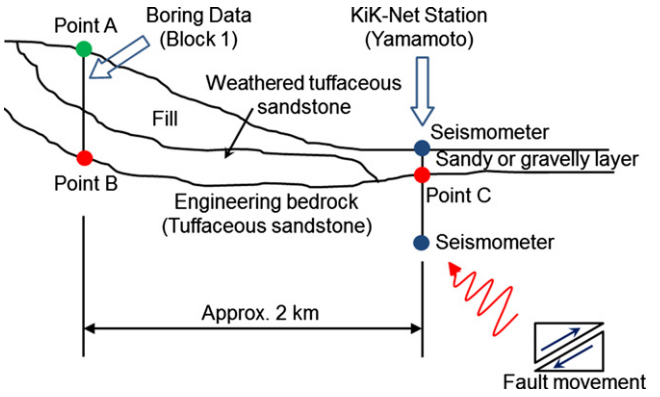

Fig. 17. Schematic diagram showing how PGA on top of fills was calculated from KiK-Net recorded motions 2 km away.

Finally, the strong motion obtained at Point C was used as input (as outcrop motion, 2E) at Point B to determine the surface acceleration at Point A. Since Points C and B are just 2 km apart, the attenuation of motion was not considered. Again, a seismic response analysis was conducted and the obtained results showed PGAs at Point A of 1322.6 and 1171.3 cm/s^2 in N–S and E–W directions, respectively. Using the equation for lateral seismic coefficient k_h, proposed by Noda et al. (1975), the obtained PGAs correspond to $k_h=0.368$ and 0.354, respectively. Note that Noda's method was based on a database consisting of accelerations ranging from 100 to 400 cm/s^2; in the absence of another available method for estimating the k_h for PGAs >1000 cm/s^2, it was deemed that this method is appropriate. Further studies are recommended to estimate the values of k_h for extremely high accelerations, such as those recorded during the 2011 earthquake.

In the pseudo-static analysis of slope stability, three cases of ground models and slip failures were considered: Case A, where the groundwater table is low (effect not considered) and the slip surfaces are composite, Case B—1, where the groundwater table is near the boundary between the fill and the sandstone and the slip surfaces are composite and Case B—2, where the groundwater table is near the boundary between the fill and the sandstone and the slip surface is circular. The applied slip surfaces were chosen based on the observed failure pattern of the block. In the analysis, the strength parameters obtained from monotonic drained triaxial tests were used.

In addition to the analysis using conventional strength parameters, a supplementary analysis was performed using the results of cyclic triaxial tests instead. In such an analysis, a two-stage approach is considered: (1) a static analysis prior to the application of the seismic load and (2) a dynamic analysis using the pseudo-static approach. In the static analysis, the strength parameters obtained from conventional tests (cohesion c and frictional angle ϕ) were used.

Table 3
Soil profile and soil properties for failed Block 1 site used in analysis.

Soil type	Depth to layer bottom (m)	H (m)	SPT N-value	γ_t (kN/m^3)	γ_{sat} (kN/m^3)	V_s (m/s)	$4H/V_s$ (s)
Fill (sandy type)	6	6	4.7	17.5	18.9	128	0.19
Tuffaceous sandstone (strongly weathered)	12	6	6.7	18.6	20.6	149	0.16
Tuffaceous sandstone (weathered)	34	22	32.4	18.6	20.6	252	0.35
				Predominant period =			0.70

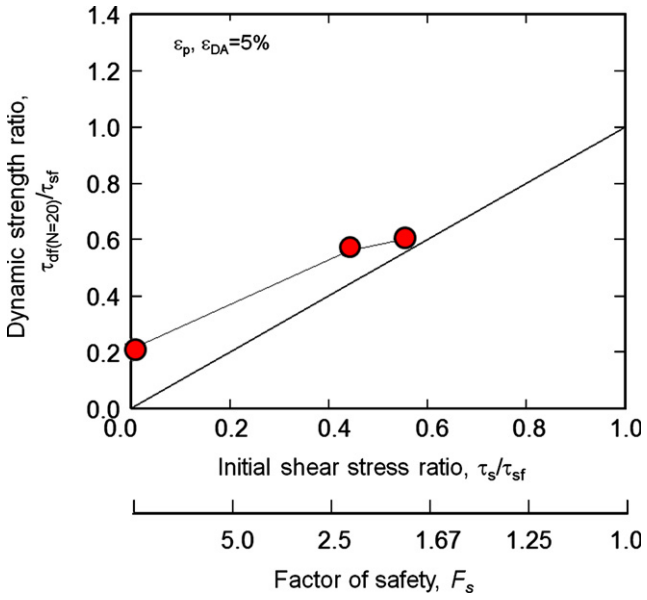

Fig. 18. Relation between dynamic strength and initial shear stress obtained from cyclic triaxial test results.

Since the calculated factor of safety, F_s, indicates the ratio of shear resistance τ_{sf} and shear stress τ_s along the slip surface (i.e., $F_s=\tau_{sf}/\tau_s$), it is possible to estimate the average static shear stress along the slip plane from the known values of F_s and τ_{sf}. From Fig. 14, the cyclic shear resistance ratios corresponding to $N=20$ cycles were read from the curves. Note that 20 cycles is usually taken as the representative number of cycles applied to define the liquefaction resistance of soils, as specified in many design codes (e.g., JRA, 1996). For earthquakes of this magnitude, however, the number of representative cycles should be large. In the absence of clear-cut guidelines on the number of representative cycles for a magnitude 9 event, $N=20$ is deemed appropriate. Moreover, looking at the gentle liquefaction resistance curves shown in Fig. 14, there is not much difference if N is taken at 20 or 100 cycles. The data read from the curves were used to plot the dynamic strength ratio, τ_{df}/τ_{sf}, as a function of the initial shear stress ratio, τ_s/τ_{sf}, as illustrated in Fig. 18. Note that $\tau_{df}=\tau_d+\tau_s$, i.e., the cyclic resistance, is added to the initial static shear stress to obtain the dynamic strength. Thus, knowing the average static shear stress along a slip plane, the corresponding dynamic strength can be estimated. This is then used to represent the soil strength in performing the pseudo-static analysis to compute the F_s for the earthquake load specified in the JRA (1999) guidelines.

In the pseudo-static analysis conducted here, yield acceleration k_y, corresponding to the limit equilibrium condition, $F_s=1.0$, was calculated. For simplicity, the value of k_y was assumed to be constant throughout the duration of the earthquake loading.

The results of the analysis are summarized in Table 4 for all the cases considered, in terms of yield acceleration k_y, necessary for the limit equilibrium condition ($F_s=1.0$), while typical model slopes and critical slip surfaces are shown in Fig. 19. For cases with composite failure surfaces, the values for the slip surfaces employed here are also indicated. Considering that the results of the above-mentioned SHAKE analysis showed k_h values of 0.35–0.37, the only condition where k_y is less than these values is the case involving the use of the dynamic strength at the slip surface (Case B-2'); all other cases using conventional strength parameters resulted in values of k_y that are higher than those induced by the 2011 earthquake. For the conventional analysis to hold, k_h should be at least 0.39 or a PGA on top of the fill should be 1,570 cm/s^2 (based on Noda's equation); this value is deemed too large.

Thus, based on the calculations presented above for the Block 1–1 site, it appears that the slope failure in Taiyo New Town can be attributed to the liquefaction of the fill, especially near the interface between the top fill layer and the highly weathered tuffaceous sandstone. With the development of excess pore water pressure, the fill underwent large deformation during the intense and prolonged shaking induced by the gigantic Tohoku earthquake. As mentioned earlier, the location of the groundwater table during the earthquake was unknown. It is possible that the groundwater table during the earthquake was above the boundary between the original ground and the fill, making the generation of excess pore water pressure during shaking viable.

Note that a slope stability analysis was performed on only one block and that further analyses are recommended for the other four sites which failed for the purpose of clarifying that liquefaction was indeed the main cause of the slope failures in Taiyo New Town. In addition, since the PGAs recorded during this event far exceed the database used in Noda's method of estimating the seismic coefficient, further studies are suggested in order to find an appropriate method for estimating k_h under large peak ground accelerations.

Table 4
Results of pseudo-static analysis for failed embankment in Block 1.

Case	Condition	Strength parameters	Yield acceleration, k_y		
			Slip 1	Slip 2	Slip 3
A	No water table; composite slip surfaces	c_d=9 kN/m^3, ϕ=31.7°	0.46	0.42	0.45
B-1	With water table; Composite slip surfaces		0.43	0.39	0.45
B-2	With water table: Circular slip surface		0.42		
B-2'	With water table: Circular slip surface	c_d=9 kN/m^3, ϕ=31.7°; then changed to dynamic strength	0.24		

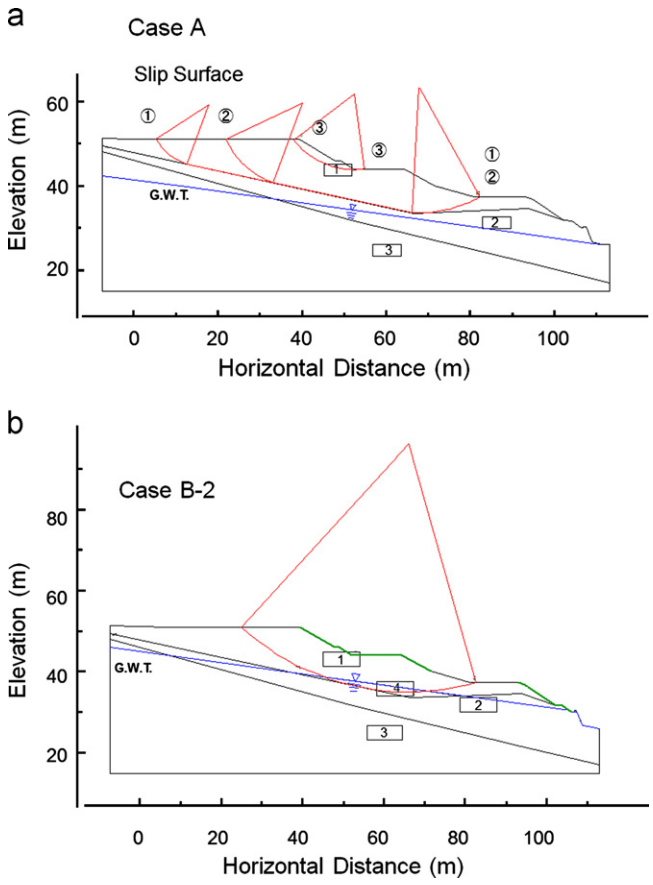

Fig. 19. Model slope with critical failure surfaces. (a) Case A (no water table with composite failure surfaces) and (b) Case B-2 (with water table and circular slip surface).

7. Conclusions

The gigantic 2011 off the Pacific coast of Tohoku Earthquake caused five slope failures in Taiyo New Town, a housing site on artificial valley fills in Yamamoto Town, Miyagi Prefecture. To understand the mechanism of the slope failures, a field inspection, a strong motion record analysis, laboratory tests, microtremor measurements and a slope stability analysis were conducted. The following are the major observations from the site investigations and the conclusions from the study presented herein:

1. The residential site of Taiyo New Town was constructed through the cut and fill method. The original hilly ground consisted of weakly consolidated tuffaceous sandstone, which showed a high degree of weathering towards the surface and manifested itself as sand on the surface. Thus, the fill material used to fill up the valleys was generally sandy soil.
2. The maximum surface acceleration recorded at the Yamamoto seismic station was 850–870 cm/s^2 with a predominant period of 4–6 Hz. The estimated maximum acceleration on top of the fills, based on the seismic response analysis, was 1170-1320 cm/s^2.
3. Each of the five slope failures at the housing site was observed to have occurred either at the edge of the artificial valley fills or at embankment sections that had been widened for road construction.
4. The sandy fill material had a fines content of F_c=20%. Even when compacted at a 90% degree of compaction, the fill material showed a very low internal friction angle and low liquefaction resistance. Moreover, the liquefaction resistance further decreased with the application of initial shear stress.
5. Microtremor measurements showed that the natural periods of the ground near the failed sites were greater than 0.5 s, indicating the large depth of the soft soil layers.
6. The pseudo-static slope stability analysis, using conventional strength parameters, could not explain the slope failure of Block 1, based on the assumption that Noda's method of estimating k_h was valid for the high PGA recorded during this earthquake. However, when the dynamic strength (or liquefaction resistance) was used to represent the soil strength at the slip surface, the yield seismic coefficient required to induce failure was lower than the estimated seismic coefficient on the fill.
7. Based on the analysis of one block, the slope failure in Taiyo New Town may be attributed to the liquefaction of the fill material induced by the intense and prolonged shaking. It is possible that during the earthquake, the groundwater level was near the boundary of the original ground and the fill, making liquefaction possible.

Acknowledgments

The authors would like to gratefully acknowledge the assistance of the engineering staff of the Yamamoto Town Office for providing access to the site for inspection and for the valuable information obtained during subsequent meetings. The strong motion data was obtained from KiK-Net.

The visit to Japan by the second author was made possible through a six-month research and study leave grant provided by the University of Auckland.

References

Fukken Gijutsu Consultant Co. Ltd., 2008. Ground Map of Built-up Residential Land, 1:25,000 scale.

Geospatial Information Agency of Japan, GSI, 2011. Area Flooded by the Tsunami (Approximate), http://www.gsi.go.jp/common/000059734.pdf. (in Japanese).

Hosono, Y., Yoshimine, M., 2004. "Liquefaction of sand in simple shear condition," In: Proceedings of the International Conference on Cyclic Behaviour of Soils and Liquefaction Phenomena, Bochum, Germany, pp. 129–136.

Hyodo, M., Murata, H., Yasufuku, N., Fujii, T., 1991. "Undrained cyclic shear strength and residual strength of saturated sand by cyclic triaxial tests,". Soils and Foundations 31 (3), 60–76.

Hyodo, M., Tanimisu, H., Yasufuku, N., Murata, H., 1994. Undrained cyclic and monotonic behavior of saturated loose sand. Soils and Foundations 34 (1), 19–32.

Hyodo, M., Orense, R., Ishikawa, S., Yamada, S., Kim, U.G., Kim, J.G., 2006. "Effects of fines content on cyclic shear characteristics of sand–clay mixtures," In: Proceedings of the Earthquake Geotechnical Engineering Workshop—Canterbury 2006, Christchurch, pp. 81–89.

Japanese Geotechnical Society, 2000. Soil Testing Procedures and Commentaries, First Revised Edition, Tokyo. (in Japanese).

Japan Road Association, JRA., 1996. "Part V: Seismic Design," Specifications for Highway Bridges. (in Japanese).

Japan Road Association, JRA., 1999. Guidelines for Safety Works on Slopes. (in Japanese).

KiK-Net, 2011. Digital Strong Motion Network, http://www.kik.bosai,go,jp/.

Nakamura, Y., 1989. A method for dynamic characteristics estimation of subsurface using microtremor on the ground surface. Quarterly Report of Railway Technical Research Institute 30 (1), 25–33.

Noda, S., Uwabe, T., Chiba, T. (1975): "Relation between seismic coefficient and ground acceleration for gravity quay wall," Report of the Port and Harbour Research Institute, 14 (4). (in Japanese).

Schnabel, P.B., Lysmer, J., Seed, H.B., 1972. SHAKE: A computer program for earthquake response analysis of horizontally layered site. EERC 1972-12 Earthquake Engineering Research Center.

Vaid, Y.P., Chung, E.K.F., Kuerbis, R.H., 1990. Stress path and steady state. Canadian Geotechnical Journal 27 (1), 1–7.